# CHAPTER 2 : SINGLE COIL DESIGN

An important component of the proximity sensor is the transducer which converts the physical distance between the sensor and the metal plate into an electrical signal that can then be manipulated by external circuitry. Two options considered for an inductive transducer were a single planar coil and a two coil planar transformer.

The first step in designing the planar inductor was to develop a technique to compute the inductance and resistance of the inductor and the mutual inductance between the plate and the inductor. Coil designs with segments at right angles were chosen. This was done to make the task of calculation simpler, since the coil could then be divided into individual segments for calculation purposes.

## 2.1.0 Resistance Calculation

The resistance of the coil was calculated using the basic formula:

$$R = \rho \frac{l}{A}, \qquad \text{Eq. (2-1)}$$

where $l$ corresponds to the length of a coil segment, $A$ is the cross-sectional area of the segment, $\rho$ is the resistivity of the material, and $R$ is the resistance of a segment. The total resistance of the coils was calculated by summing the resistance of the individual segments that make up the coil. Note that the resistance calculated is the D.C. resistance of the coil and does not take into account phenomena such as current redistribution due to proximity effects and the skin depth effect, both of which cause the resistance to increase with frequency. Also the effect of current crowding at corners is not included.

### 2.2.0 Coil Inductance Calculation

A number of papers have been written [3][5][6][14][18], giving formulae to calculate the inductance of a planar coil. However as shown by Greenhouse [7], his method based on Grover's model [8][9] is perhaps the most accurate and comprehensive.

Rosa [16][17] and Grover developed the concept of the "mutual inductance" between two segments and the "self-inductance" of a segment. The **mutual inductance** between two segments is defined as the flux linkages in segment 1 due to unit current in segment 2 or visa-versa. Note if the currents in the two segments are flowing in the opposite directions, the mutual inductance is negative and if the currents are flowing in the same direction, the mutual inductance is positive. In the absence of magnetic materials, mutual and self-inductances are parameters that are independent of the value of the current and depend only on the geometry of the system.

The **self-inductance** of a segment is defined as the mutual inductance of two parallel straight filaments of infinitesimal width, spaced at the *geometric mean distance* of all the points of the segment from each other. The geometric mean distance is the average of the logarithm of the distance between all the pairs of points that make up the segment. The self-inductance is thus a special case of mutual inductance.

Greenhouse used these concepts to calculate the inductance of the rectangular spiral inductor. He divided the rectangular coils into segments and calculated the self-inductance of the individual segments. The total self-inductance of the coil was the sum of the self-inductances of the individual segments.

Now the mutual inductance between segments was calculated. Since the coil was rectangular, only pairs parallel to each other were considered. If the segments had opposing currents, the mutual inductance was calculated as a negative number, while the

mutual inductance of segments with currents flowing in the same direction was calculated as a positive number. The segments which are at right angles to each other do not interact (their mutual inductance is zero). This is because the mutual inductance between two segments is proportional to the “dot product” of the vector magnetic potential produced in one segment and the length of the other [10], as shown in Eq. (2-2).

$$M_{i,\,j} = \frac{\int A_j \bullet dl_i}{I_j}, \qquad \text{Eq. (2-2)}$$

where $M_{i,\,j}$ is the mutual inductance between segment ‘i’ and segment ‘j’, $A_j$ is the vector magnetic potential of segment ‘j’ integrated over the length of segment ‘i’, and $I_j$ is the current flowing in segment ‘j’. The direction of $A_j$ is parallel to the direction of the length of segment ‘j’. Thus if segment ‘j’ is at right angles to segment ‘i’, the numerator in Eq. (2-2) is equal to zero.

The algebraic sum of the total of the self-inductance and the negative and positive mutual inductance corresponds to the low frequency inductance of the coil. A schematic of a planar coil with individual segments numbered from 1 to 5, is shown in Fig. (2-1). The arrows correspond to the direction of the flow of current in the segments.

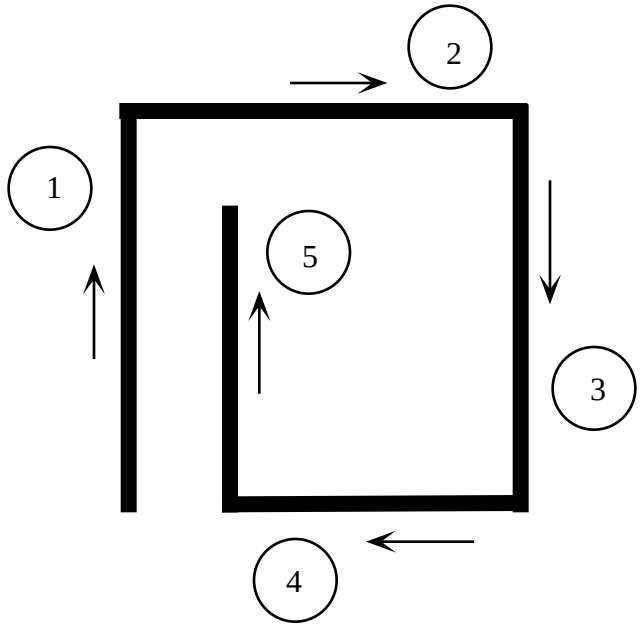


**Fig. (2-1): Explanation of Greenhouse's model.**

Thus for Fig. (2-1) shown above, the total inductance, $L_{tot}$, is:

$$L_{tot} = L_1 + L_2 + L_3 + L_4 + L_5 - 2\,(M_{1,3} + M_{2,4} + M_{3,5}) + 2M_{1,5}, \qquad \text{Eq. (2-3)}$$

where $L_i$ is the self-inductance of segment 'i', and $M_{i,j}$ is the mutual inductance between segments 'i' and 'j'. The factor of 2 appears because the flux linkages produced in segment 'i' due to current in segment 'j' and the flux linkages produced in segment 'j' due to current in segment 'i' are equal due to reciprocity.

Using the equations derived by Rosa [16][17] and Grover [8][9],

$$L_i = 0.002 l_i \left( \ln\left( \frac{2l_i}{GMD} \right) - 1.25 + \frac{AMD}{l_i} + \frac{\mu}{4} T \right) \quad \text{Eq. (2-4)}$$

$$M_{i,j} = 0.002 l Q \quad \text{Eq. (2-5)}$$

$$Q = \ln \left\{ \frac{l}{GMD} + \left[ 1 + \left( \frac{l}{GMD} \right)^2 \right]^{\frac{1}{2}} \right\} - \left[ 1 + \left( \frac{GMD}{l} \right)^2 \right]^{\frac{1}{2}} + \frac{GMD}{l} \quad \text{Eq. (2-6)}$$

$$GMD = \ln(d) - \{ \left[ \frac{1}{12} \left( \frac{d}{w} \right)^2 \right] + \left[ \frac{1}{60} \left( \frac{d}{w} \right)^4 \right] + \left[ \frac{1}{168} \left( \frac{d}{w} \right)^6 \right] + \left[ \frac{1}{360} \left( \frac{d}{w} \right)^8 \right] + \left[ \frac{1}{660} \left( \frac{d}{w} \right)^{10} \right] + \ldots\ldots \} \quad \text{Eq. (2-7)}$$

$$AMD = w + t, \quad \text{Eq. (2-8)}$$

where $L_i$ is the self-inductance of segment 'i' in μH, $M_{i,j}$ is the mutual inductance between segments 'i' and 'j' in μH, $l_i$ is the length of the segment 'i' in centimeters, $\mu$ is the relative permeability of the conductor, $T$ is the frequency correction factor (= 1 for low frequencies), $d$ is the distance between conductor filaments in centimeters, $w$ is the width of the conductor in centimeters, $t$ is the thickness of the conductor in centimeters, $Q$ is the mutual inductance parameter, $GMD$ is the Geometric Mean Distance, and $AMD$ is the Arithmetic Mean Distance.

Ruehli [20] has shown that Eq. (2-2) can also be written as:

$$M_{i,j} = \frac{\int_{S_i} B_j \bullet ds_i}{I_j}, \qquad \text{Eq. (2-9)}$$

where $M_{i,j}$ is the mutual inductance between segment ‘i’ and ‘j’, $B_j$ is the flux density due to current in segment ‘j’, $I_j$ is the current in segment ‘j’, and $S_i$ is the area bounded by segment ‘i’ and infinity and by straight lines that are located at the ends of segment ‘j’ and are perpendicular to segment ‘j’. The magnetic flux density due to a current on a finite length filament can be obtained with the Biot-Savart law [19]. Integrating the equation given above gives us Eq. (2-5). Since the self-inductance is a special case of the mutual inductance obtained by substituting the GMD of the distance between segments by the GMD of the cross section of a segment, the self-inductance formula shown in Eq. (2-4) can be obtained.

To calculate the mutual inductance between two segments of different lengths (j and m, where j > m), as shown in the Fig. (2-2) (note that the current in both the segments is flowing in the direction of the plane of the paper),

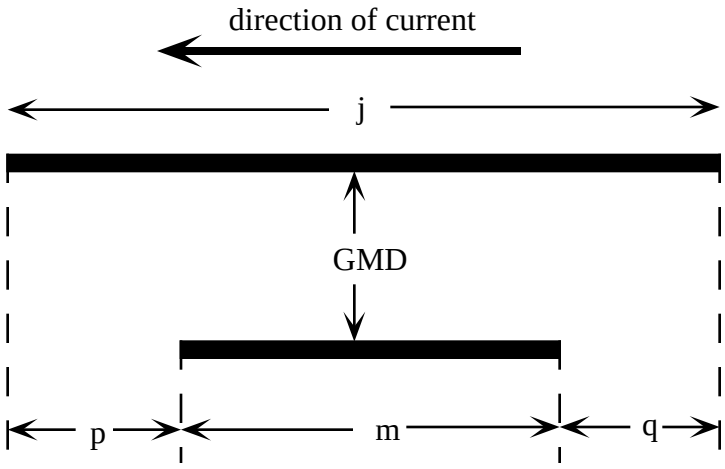


**Fig. (2-2): Calculation of the mutual inductance between two segments of different lengths.**

$$2M_{j,m} = (M_{m+p} + M_{m+q}) - (M_p + M_q)\,, \qquad \text{Eq. (2-10)}$$

where

$$M_{m+p} = 2\,(m+p)\,Q_{m+p}\,. \qquad \text{Eq. (2-11)}$$

## 2.3.0 Calculation of Mutual Inductance between Plate and Coil

As explained in the introduction to the chapter, the single planar coil forms the transducer of the proximity sensor. The proximity sensor measures the distance between itself and a metal plate. Since the plate is a conductor itself, there is a mutual inductance produced between the coil and the plate. The method of images [2][11][12] was used to calculate the mutual inductance between the coil and the plate. This method assumes that the plate is a “good” conductor and infinite in extent. Image theory

replaces the system of a plate and a coil with a coil and it's image. As shown in Fig. (2-3), the image is placed below the surface of the metal at a distance equal to the distance between the coil and the plate surface and the direction of the current (flowing perpendicular to the plane of the page) in the image is opposite to that flowing in the coil. Also the magnitude of the current in the image is assumed to be equal to the magnitude of the current in the actual coil. This can be done by imaging the supply which drives the coil in the plate. Note that the image theory is valid only for high frequencies or when the resistivity is zero.

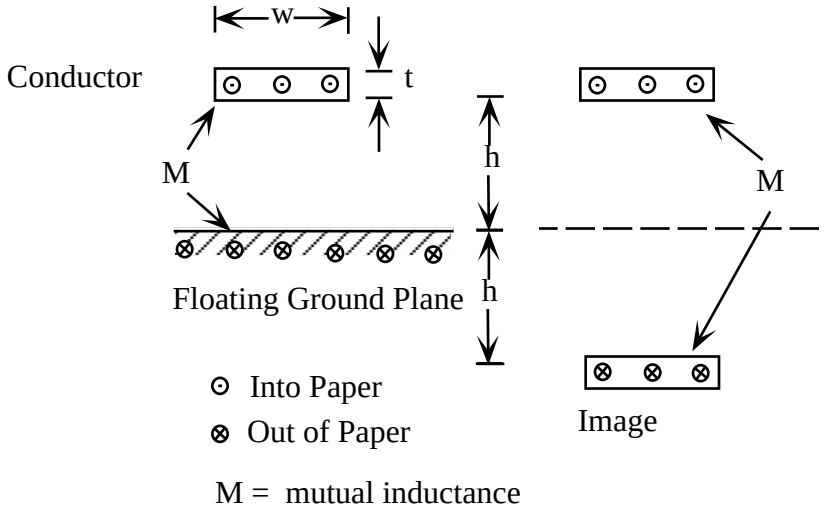


**Fig. (2-3): A conductor over a ground plane is replaced by the conductor and it's image. M is the mutual inductance between the conductor and the ground plane, which equal to the mutual inductance between the conductor and it's image.**

As shown in Fig. (2-4), the mutual inductance between the coil and it's image was calculated based on Rosa's formulae [17] for the GMD of two strips. The currents in this diagram are flowing perpendicular to the page.

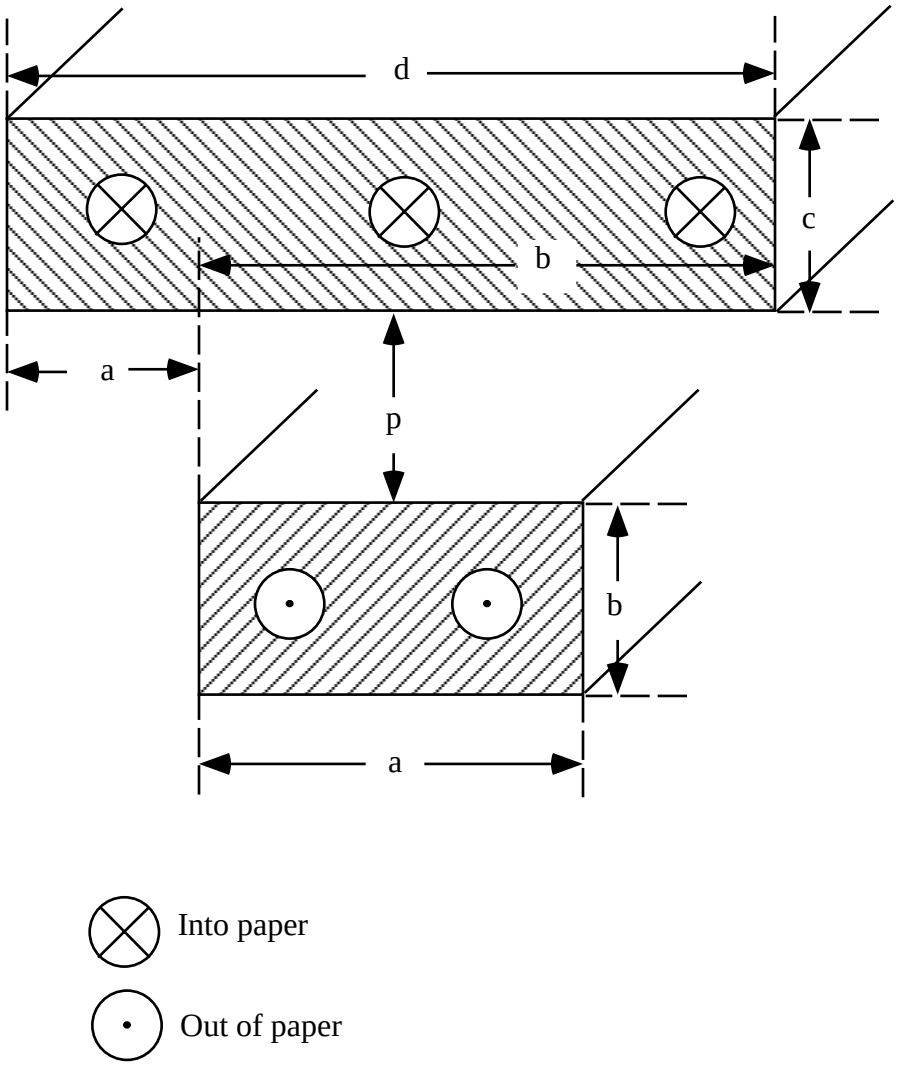


**Fig. (2-4): Model for Rosa's calculation of GMD between two segments of different cross section.**

$$abcd\log GMD = \qquad \text{Eq. (2-12)}$$

$$\frac{1}{4}\left[ (p+b+c)^2 \left\{ \beta^2 - \frac{(p+b+c)^2}{6} \right\} \right] \log\left( (p+b+c)^2 - \beta^2 \right)$$
$$- \frac{1}{4}\left[ (p+b)^2 \left\{ \beta^2 - \frac{(p+b)^2}{6} \right\} \right] \log\left( (p+b)^2 - \beta^2 \right)$$
$$- \frac{1}{4}\left[ (p+c)^2 \left\{ \beta^2 - \frac{(p+c)^2}{6} \right\} \right] \log\left( (p+c)^2 - \beta^2 \right)$$
$$+ \frac{1}{4}\left[ p^2 \left\{ \beta^2 - \frac{p^2}{6} \right\} \right] \log\left( p^2 - \beta^2 \right)$$

$-$ (the same series of terms with $\beta$ replaced by $\alpha$)

$$+ \frac{\beta}{3}(p+b+c)^3 \operatorname{atan}\frac{\beta}{p+b+c} + \frac{\beta^3}{3}(p+b+c)\operatorname{atan}\frac{(p+b+c)}{\beta}$$
$$- \left( \frac{\beta}{3}(p+b)^3 \operatorname{atan}\frac{\beta}{p+b} + \frac{\beta^3}{3}(p+b)\operatorname{atan}\frac{(p+b)}{\beta} \right)$$
$$- \left( \frac{\beta}{3}(p+c)^3 \operatorname{atan}\frac{\beta}{p+c} + \frac{\beta^3}{3}(p+c)\operatorname{atan}\frac{(p+c)}{\beta} \right)$$
$$+ \frac{\beta}{3}p^3 \operatorname{atan}\frac{\beta}{p} + \frac{\beta^3}{3}p\operatorname{atan}\frac{p}{\beta}$$

$-$ (the same series of terms with $\beta$ replaced by $\alpha$)

$$- \frac{(\beta-\alpha)}{8}\left\{ (p+b+c)^2 - (p+c)^2 - (p+b)^2 + p^2 \right\} - \frac{11}{6}abcd$$

where

$$\alpha = \frac{1}{2}(d-a)\,, \qquad \text{Eq. (2-13)}$$

$$\beta = \frac{1}{2}(d+a)\,, \qquad \text{Eq. (2-14)}$$

$GMD$ is the Geometric Mean Distance, and dimensions $a$, $b$, $c$, and $d$ are as shown in the Fig. (2-4).

## 2.4.0 Measurements

To verify the simulation results, three coils were fabricated on a copper printed circuit board (PCB). The three designs are shown in Fig. (2-5). All the coils had $l_1 = l_2 = 1$ cm. The coils had a line width of approximately 0.03 cm. The separation between adjacent lines was also approximately 0.03 cm. The copper on the PCB was 17 μm thick. Large pads were chosen so as to decrease the contribution of the contacts to the measured inductance and resistance. For the spiral coil, a copper wire was soldered from the center to the pad to complete the circuit.

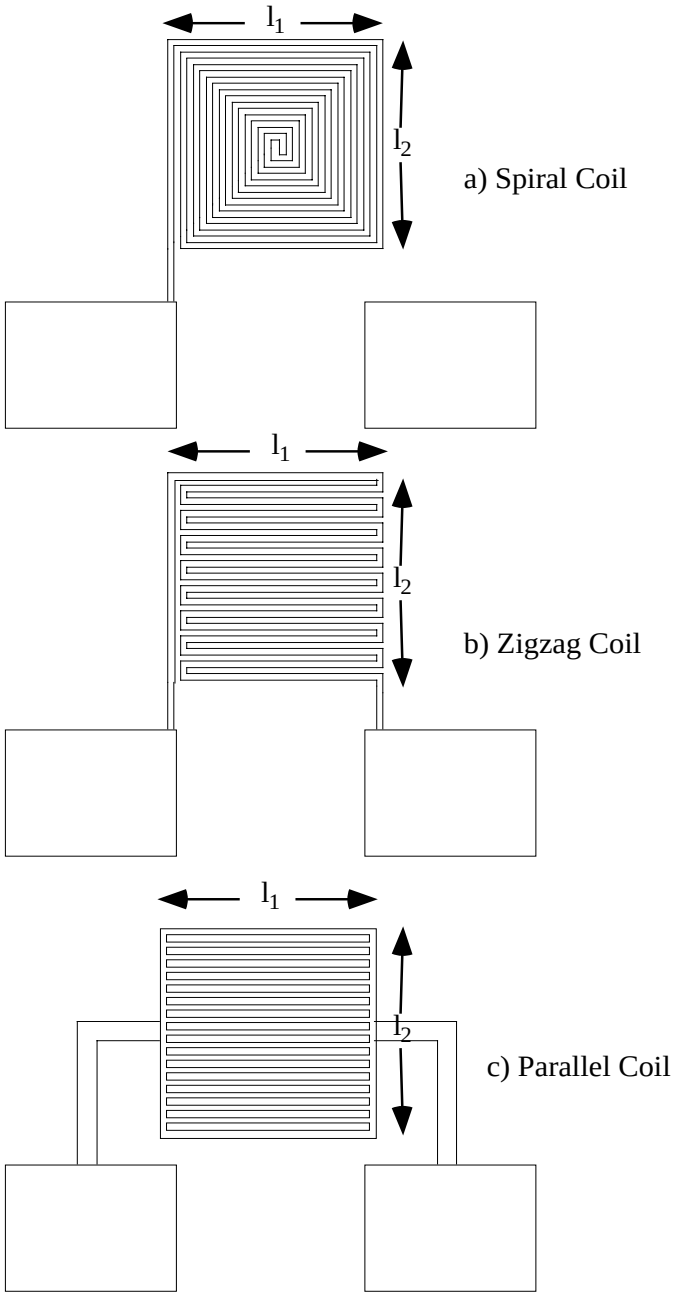


**Fig. (2-5): Single coil mask designs.**

The series resistance and the series inductance of the coils was measured for frequencies from 10 kHz to 40 MHz using the HP4194A Impedance/Gain-Phase Analyzer. Experiments to simulate the impact of a variable gap between the coils and the plate were performed (a copper PCB of dimensions 4 cm x 4 cm x 17 μm was used as the plate). Glass coverslips ($\text{thickness} \cong 0.015\ \text{cm}$) and a glass slide ($\text{thickness} \cong 0.125\ \text{cm}$) were inserted between the coil and the plate to simulate different gaps and to ensure that the distance between the coil and the metal plate was uniform over the whole coil surface. To eliminate the effect of the pads, a "compensating short" was measured first (shown in Fig. (2-6)) and it's inductance and resistance were subtracted from the inductance and resistance data for the other coils. The short essentially compensates for the self-inductance of the pads and the short length of conductors which connects the pads to the actual coil. The mutual inductance between the pads and the segments which form the coil is not compensated for. However this mutual inductance is a small value due to the large distance between the segments and the pads and the large width of the pads.

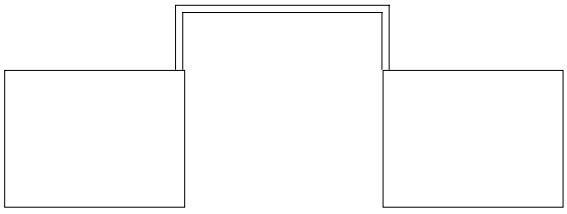

**Fig. (2-6): Compensating short to eliminate the effect due to the contact pads.**

In Fig. (2-7) to Fig. (2-9) the solid lines ( ——— ) on all the graphs correspond to the inductance and resistance of the coils with no metal plate (or equivalently, the metal plate at infinity). The dashed lines ( — — ) correspond to the case where the

distance between the metal plate and the coil is approximately 0.125 cm (a glass slide placed between the coil and the metal plate). The dotted lines ( ····· ) correspond to the case where the distance between the coil and the metal plate is approximately 0.015 cm (a coverslip placed between the coil and the metal plate).

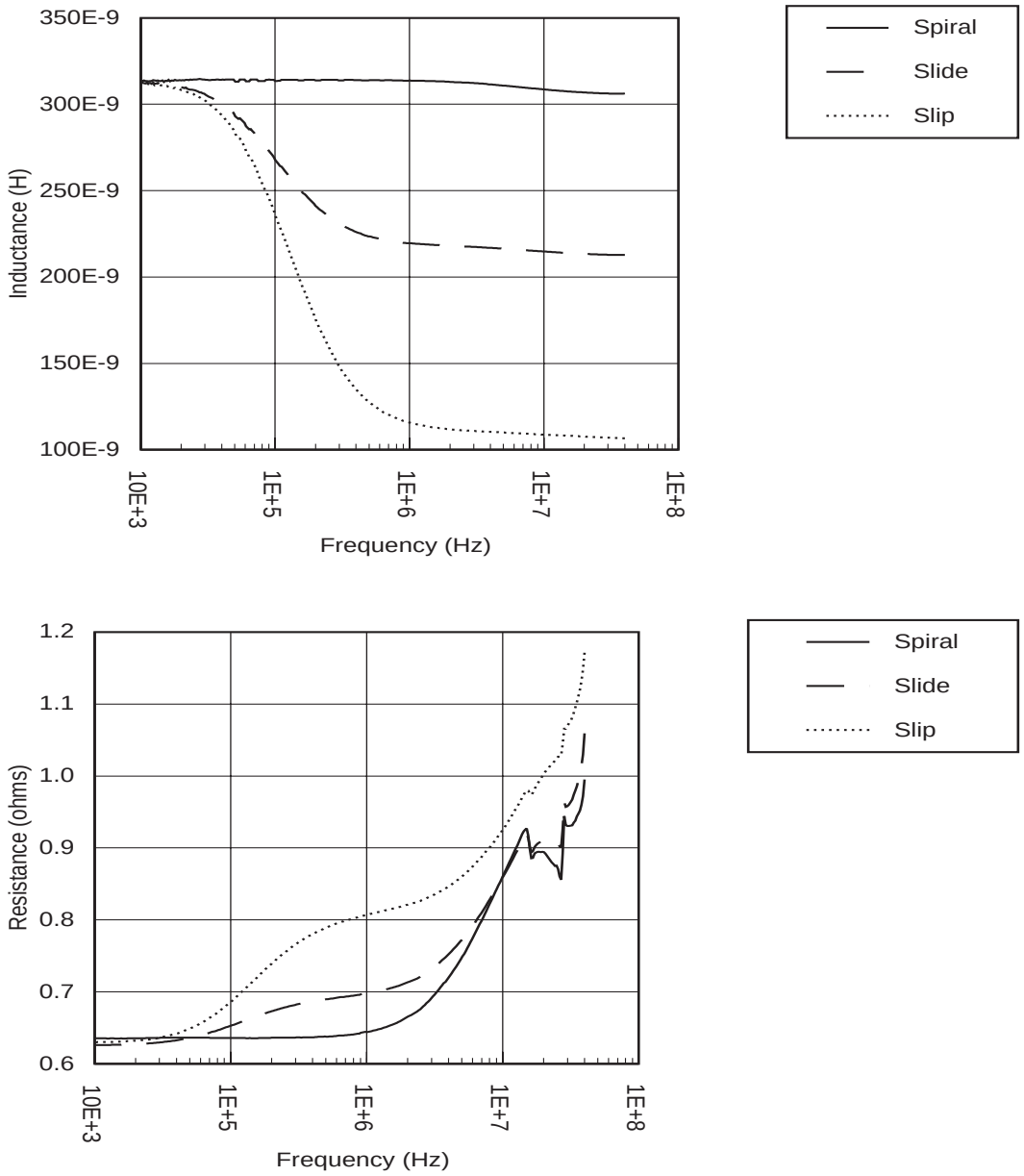


**Fig. (2-7): Inductance and resistance graphs for the spiral coil.**

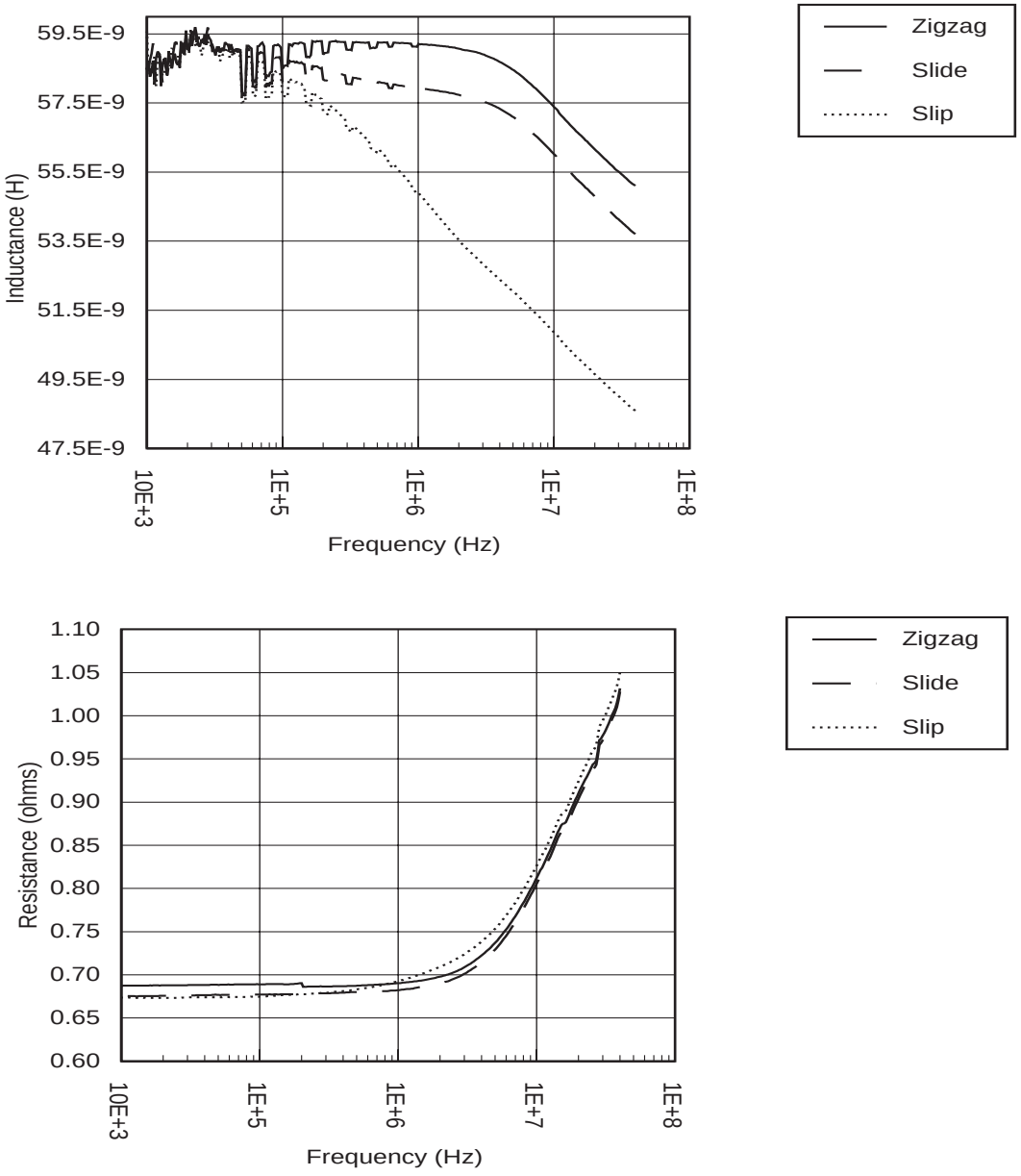


**Fig. (2-8): Inductance and resistance graphs for the zigzag coil.**

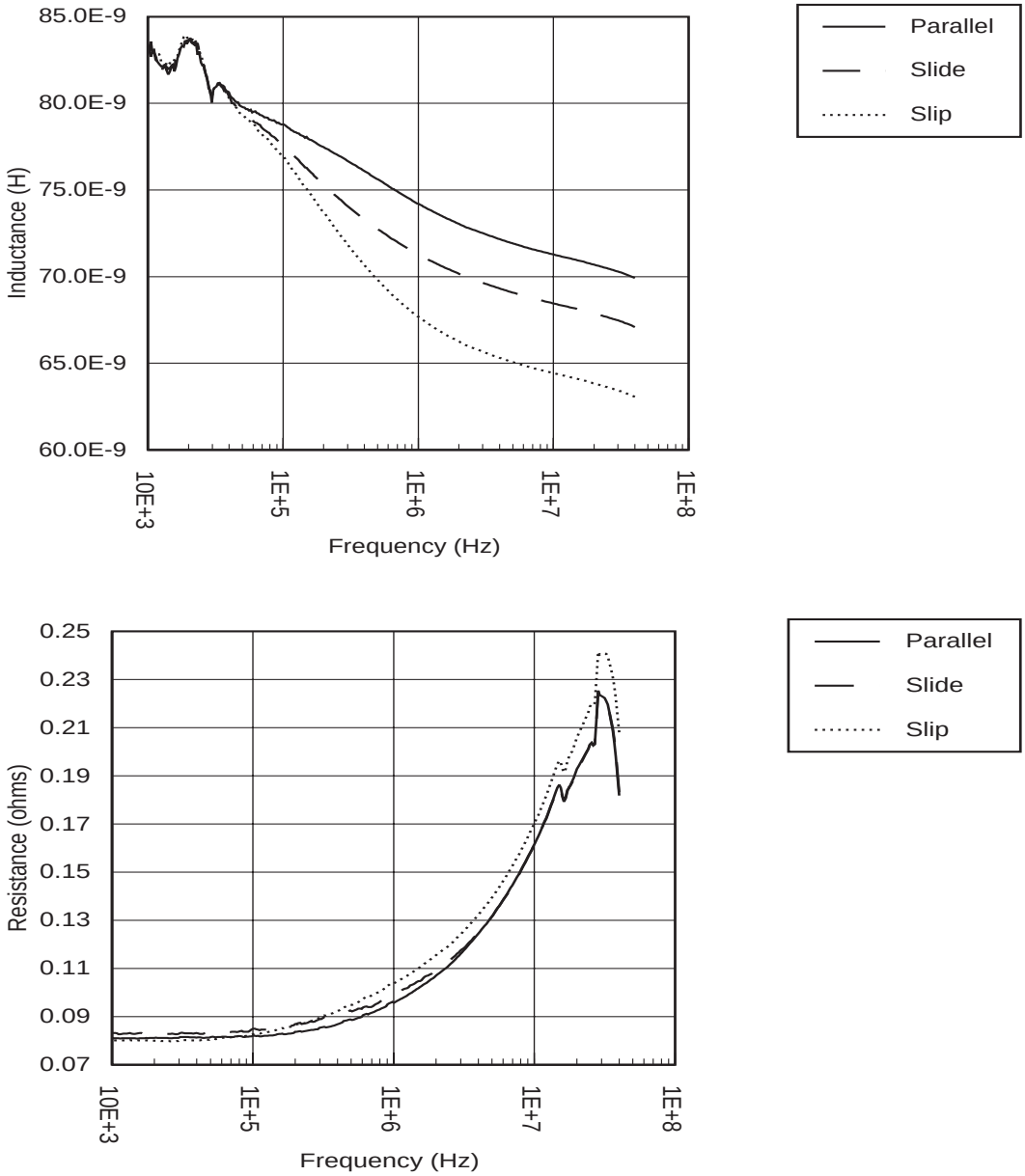


**Fig. (2-9): Inductance and resistance graphs for the parallel coil.**

As can be seen from the graphs, for the same amount of area (1 $cm^2$) and minimum line width (0.03 cm), the magnitude of the inductance of the three coils is different. The spiral coil shows the largest inductance while the zigzag coil shows the smallest. The large inductance of the spiral coil is due to the large number of closely spaced conductors carrying current in the same direction causing the mutual inductance between the segments to be added to the self-inductance. Similarly the low inductance of the zigzag coil is due to the large number of closely spaced conductors carrying current in opposite directions causing the mutual inductance between segments to be subtracted from the self-inductance.

All the coils (without the plate) show a slight decrease in the inductance and a large increase in resistance with frequency. This is due to the rearrangement of the current flow in the segments due to proximity effects and skin effects [4]. The effect causes the current to crowd towards the edges of the segment.

The inductance of the system (coil plus plate) decreases as the plate is brought closer to the coil. This is due to the increased mutual inductance between the plate and the coil.

The three coils show different amounts of absolute change with the same gap. The Spiral Coil shows the largest absolute change in inductance (approximately 30% for the “slip” case) compared to the Zigzag and Parallel Coils (both show an approximately 10% change for the “slip” case).

In the case of the spiral coil, we can easily measure distances equal to approximately 5 times (0.15 cm) the separation between the segments (0.03 cm which is also equal to the width of the segment). For distances larger than 5 times the separation, the change in inductance with distance becomes non-linear as the inductance of the system - coil

and plate - approaches the inductance with the plate at infinity).

The inductance of the system (coil and plate) is frequency dependent. This can be explained by using a transformer model to represent the coil and the plate as shown in Fig. (2-10). The coil forms the primary coil and the plate forms the secondary.

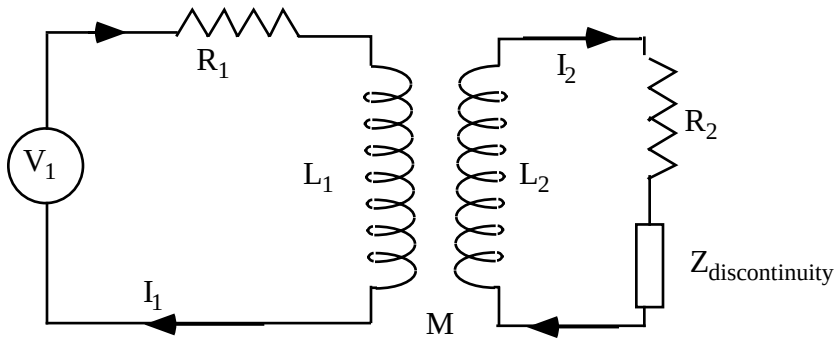


**Fig. (2-10): Single coil transformer to represent the coil and plate system. $R_1$ and $L_1$ represent the coil, $R_2$ and $L_2$ represent the plate and $Z_{discontinuity}$ represents the discontinuity in the current flow in the plate.**

For the transformer shown in Fig. (2-10), $L_1$ and $R_1$ correspond to the inductance and resistance of the coil, respectively. $L_2$ and $R_2$ correspond to the inductance and resistance of the plate. $Z_{discontinuity}$ is the discontinuity in the current flow in the plate since the current in the plate does not have a closing path. This discontinuity will be discussed further in a section 2.5.0. Writing the Kirchoff's current loop equations for the circuit given above,

$$V_1 = I_1 (R_1 + j\omega L_1) - I_2 (j\omega M) , \qquad \text{Eq. (2-15)}$$

$$0 = -I_1(j\omega M) + I_2(R_2 + j\omega L_2), \qquad \text{Eq. (2-16)}$$

Rearranging terms, we get

$$\frac{V_1}{I_1} = \left[R_1 + \frac{\omega^2 M^2 R_2}{R_2^2 + \omega^2 L_2^2}\right] + j\omega\left[L_1 - \frac{\omega^2 M^2 L_2}{R_2^2 + \omega^2 L_2^2}\right], \qquad \text{Eq. (2-17)}$$

As can be seen, the coefficients of the real and imaginary parts are frequency dependent. For low frequencies, the resistance and inductance are almost equal to $R_1$ and $L_1$ respectively. For high frequencies, ($\omega L_2 \gg R_2$), the $\omega^2$ terms cancel, and the inductance settles to a lower value of

$$L_{effective} = L_1 - \frac{M^2}{L_2}, \qquad \text{Eq. (2-18)}$$

while the resistance settles at a higher value of

$$R_{effective} = R_1 + \frac{M^2 R_2}{L_2^2}. \qquad \text{Eq. (2-19)}$$

In a conductor, an increase in resistance with frequency can be attributed to two reasons. The first is due to the decrease in the skin depth of the conductor with frequency and the second is due to the effect of other conductors in close proximity with the conductor. This ‘proximity effect’ is related to the magnetic fields produced by the currents flowing in the other conductors affecting the current distribution in the original

conductor. The current in the conductor distributes towards the edges of the conductor with an increase in frequency.

For copper, the skin depth at 40 MHz is approximately 10.5 μm. This means that for the skin depth effect to be significant, the thickness of the conductor needs to be greater than 21 μm (two times the skin depth). Since the coils are made from copper that is only 17 μm thick this effect is not important for the range of frequencies measured. However, since the coils are made of segments in close proximity to each other, the proximity effect does affect the resistance of the coils. In the case of the zigzag coil and the parallel coil the proximity effect dominates the resistance term and hence the resistance continues to increase at higher frequencies. For the spiral coil however a distinct “bump” is seen due to the resistance trying to settle down to the higher value and then continuing to increase due to the proximity effect.

### 2.4.1 Image theory revisited

As explained in section 2.3.0, at high frequencies (or for a perfect conductor), a conductor placed over a ground plane can be replaced by a conductor and it’s image since the mutual inductance in both the cases is equal. By the image theory, the circuit model used to represent the coil and the plate is shown in Fig. (2-11).

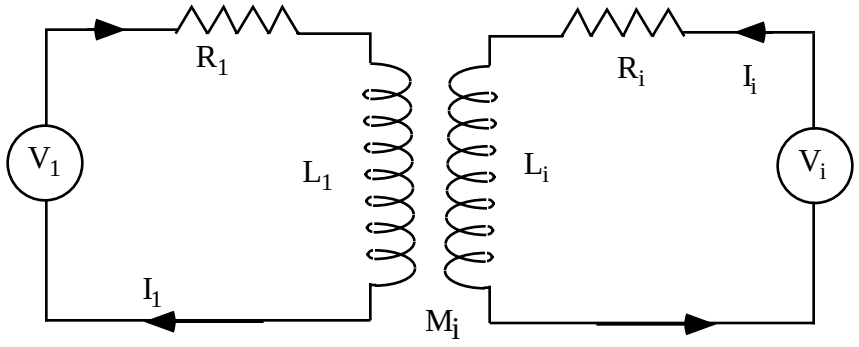


**Fig. (2-11): Circuit model for image theory.**

This circuit shows the image of the coil and the image of the supply too. Here $V_1 = V_i$, $L_1 = L_i$ and $R_1 = R_i$, where $V_i$, $L_i$ and $R_i$ are the image supply voltage, image inductance, and image resistance, respectively. Due to the situation shown above the currents in the two circuits are equal, i.e. $I_1 = I_i$. The imaginary part of the input impedance in this case is,

$$L_{effective} = L_1 - M_i . \qquad \text{Eq. (2-20)}$$

Equating the inductance equations Eq. (2-18) and Eq. (2-20), we get

$$M_i = \frac{M^2}{L_2} . \qquad \text{Eq. (2-21)}$$

As shown in Fig. (2-12) a conductor segment over a “ground” plane can be connected in two different ways. The arrows represent the direction of the flow of current. Note

that the component values, including the mutual inductance, ideally should not depend upon the connection. Alongside the connection diagram is the transformer model for the two connection schemes.

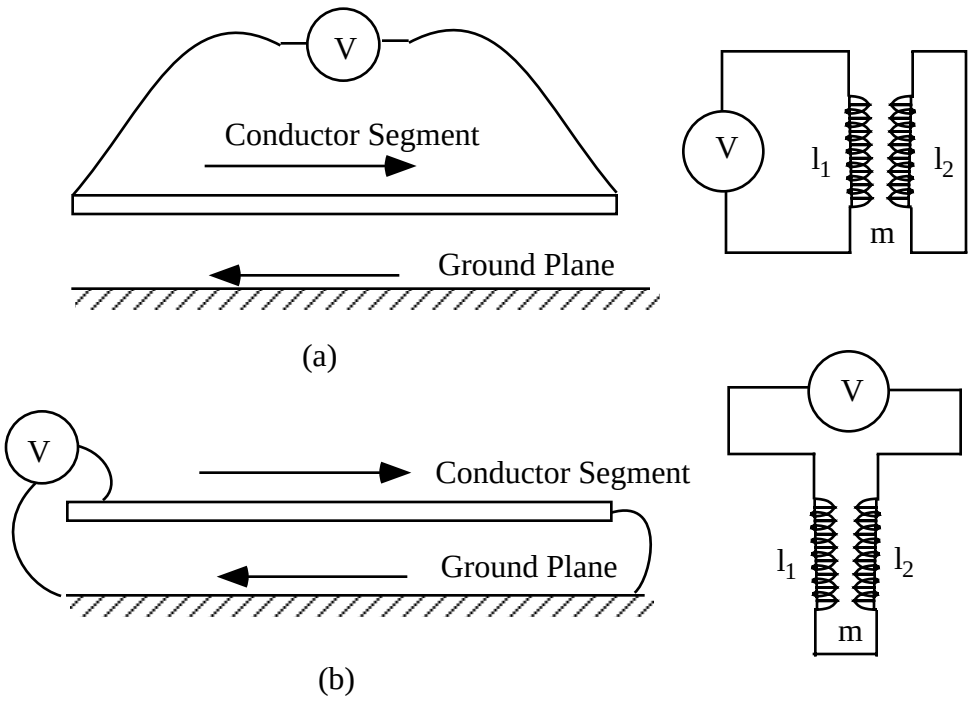


**Fig. (2-12): Connection schemes for the transformer model.**

For both the cases shown above, using image theory for Fig. (2-12)a and the formulae tabulated by Rostek [18] for Fig. (2-12)b, the value of the inductance is $l_1 - M_i$ where $M_i$ is the mutual inductance between the conductor and it's image. However using Kirchoff's current law for the two transformer models shown, the values of the (high frequency) inductance in the two cases is:

$l_1 - \frac{m^2}{l_2}$ for Fig. (2-12)a and, Eq. (2-22)

$l_1 + l_2 - 2m$ for Fig. (2-12)b. Eq. (2-23)

Equating equations Eq. (2-22) and Eq. (2-23), we have:

$l_1 - M_i = l_1 - \frac{m^2}{l_2}$ and Eq. (2-24)

$l_1 - M_i = l_1 + l_2 - 2m$. Eq. (2-25)

Thus,

$\frac{-m^2}{l_2} = l_2 - 2m$. Eq. (2-26)

Rearranging terms we get,

$l_2 = m$. Eq. (2-27)

Also from the Image theory and transformer equations for Fig. (2-12)a,

$M_i = m$. Eq. (2-28)

This implies that for Fig. (2-10) and Fig. (2-11), $M_i = M = L_2$.

### 2.4.2 Conclusions from Measurements

Based on these results, the rectangular spiral coil shows the highest inductance and also the largest change in inductance with gap. Thus the rectangular spiral coil may be the best design choice. The disadvantage of the rectangular spiral coil is that an air bridge is needed to connect the center of the coil to one of the leads. A non-crossing coil design would solve this problem.

Since the spiral coil seemed to be the best choice, all simulations were based on the spiral geometry. The coil had $l_1 = l_2 = 1$cm. The line width was approximately 0.03 cm with the separation between adjacent lines also equal to approximately 0.03 cm. The coil was 17 μm thick. The program calculated the inductance of the spiral to be 315 nH. With the glass-slide (0.125 cm) the inductance dropped to 222 nH and with the cover-slip (0.015 cm) the inductance dropped further to 105 nH. As can be seen from the inductance graph for the spiral coil (Fig. (2-7), p.27), these are very close to the experimental results in the higher frequency region where the inductance is simply $L_1 - M_i$. A graph of the comparison between the experimental data and calculated results is given in Fig. (2-13).

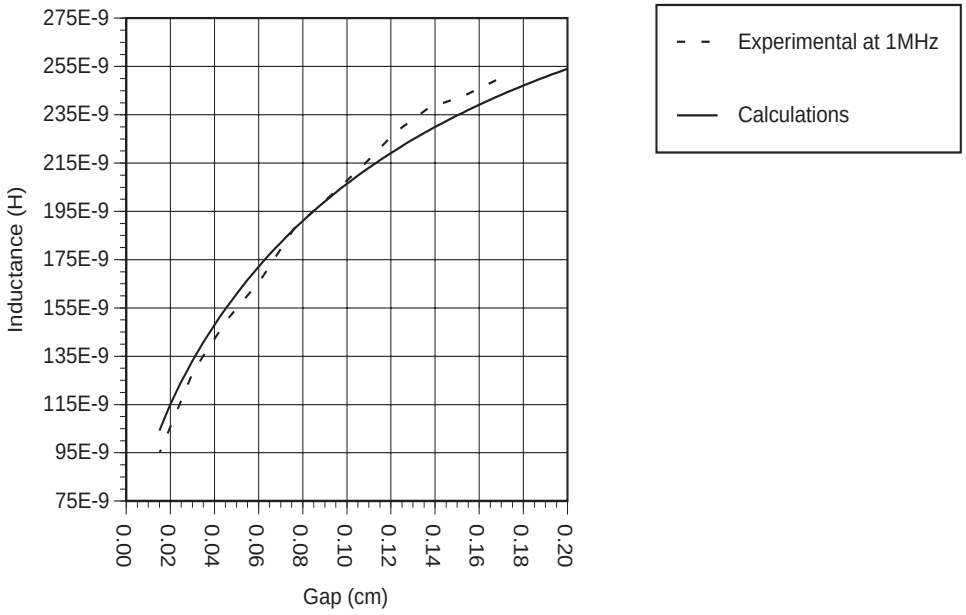


**Fig. (2-13): Experimental data vs. calculation results for inductance vs. gap**

## 2.5.0 The Discontinuity

Shown in Fig. (2-14) is a coil with it's image in the floating metal plate. The coil with the voltage source forms a closed current loop. However in the case of the image, the current (which flows in the opposite direction to that in the coil) has to "jump" from point 'a' to point 'b' in order to complete the current loop. This discontinuity adds a small resistance and inductance to that of the image. Experiments were carried out in order to investigate the properties of the discontinuity.

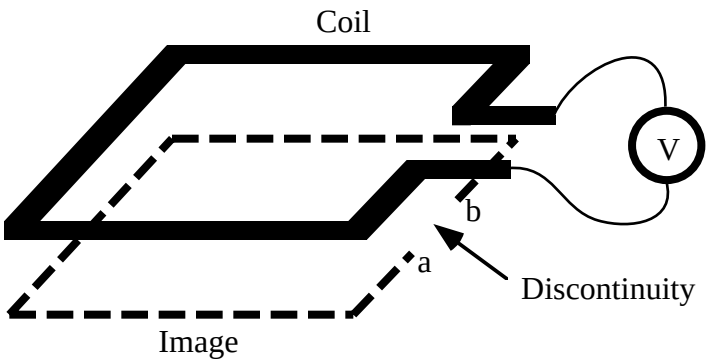


**Fig. (2-14): Coil with it's image and the discontinuity.**

First a spiral coil as shown in Fig. (2-15) was fabricated. This coil, however, had fewer turns so that there was a larger area in the center of the coil without segments (this is the reason for the reduced inductance and resistance compared to the earlier spiral coil). Next the inductance of the coil was measured with the metal plate at a distance of a cover-slip (thickness $\cong 0.015$ cm). The experiment was repeated with a "small" slit in the metal plate. The slit was "small" so that it lay in the "discontinuity" region without cutting any of the image segments. Theoretically this meant that the current would not be able to take the shortest route from point 'a' to point 'b' (in Fig. (2-14)). The experiment was repeated again, this time with a "long" slit. The slit this time was "long" enough that it actually cut some of the image segments. Now the current would have to take an even longer route from point 'a' to point 'b'.

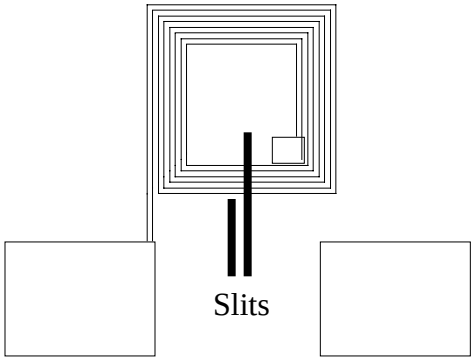


**Fig. (2-15): Reduced coil showing position of slits in the metal plate with respect to the coil**

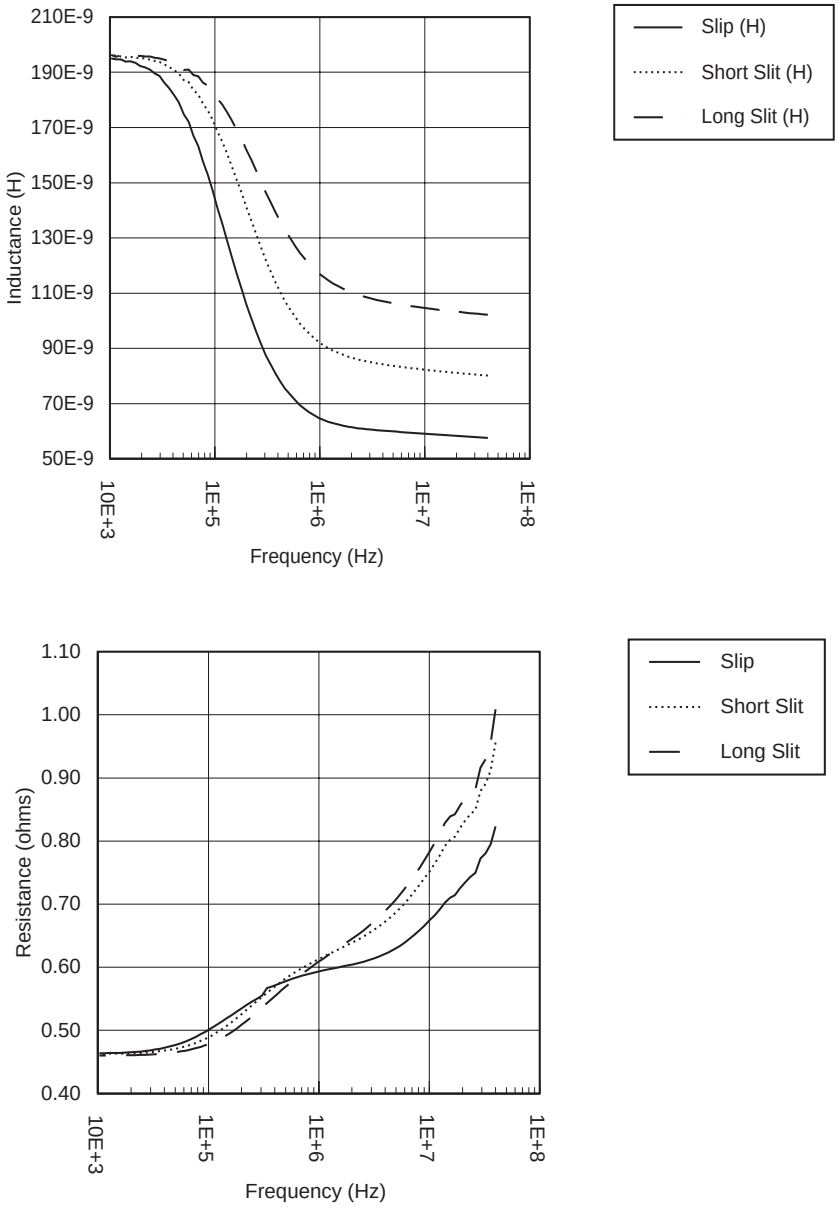


**Fig. (2-16): Inductance and resistance graphs for discontinuity.**

Fig. (2-16) shows the inductance and resistance graphs for the slit experiment. As can be seen from the graph, the presence of the slit does affect the behavior of the coil and

plate system. The inductance graph shows that the mutual inductance (and hence the secondary inductance) decreases as the slit is made longer. Also since there is a slight shift in the position where the curve flattens out (it occurs at a slightly higher frequency as the slit is made longer) we can infer that there is an increase in the image resistance. This inference is corroborated by the resistance graph which shows a higher rate of increase in resistance at higher frequencies.

## 2.6.0 Effect of change in Dielectric between the Coil and the Metal Plate

In order to determine the effect of change in the response if the dielectric between the coil and the metal plate were changed, the inductance of the coil was measured with two different dielectrics (glass and a dielectric with the $\varepsilon_r = 10.5$). Note that the thickness of the dielectric was approximately equal to 0.075 cm or 5 coverslips. Given below in Fig. (2-17), are the inductance and resistance graphs for the experiment.

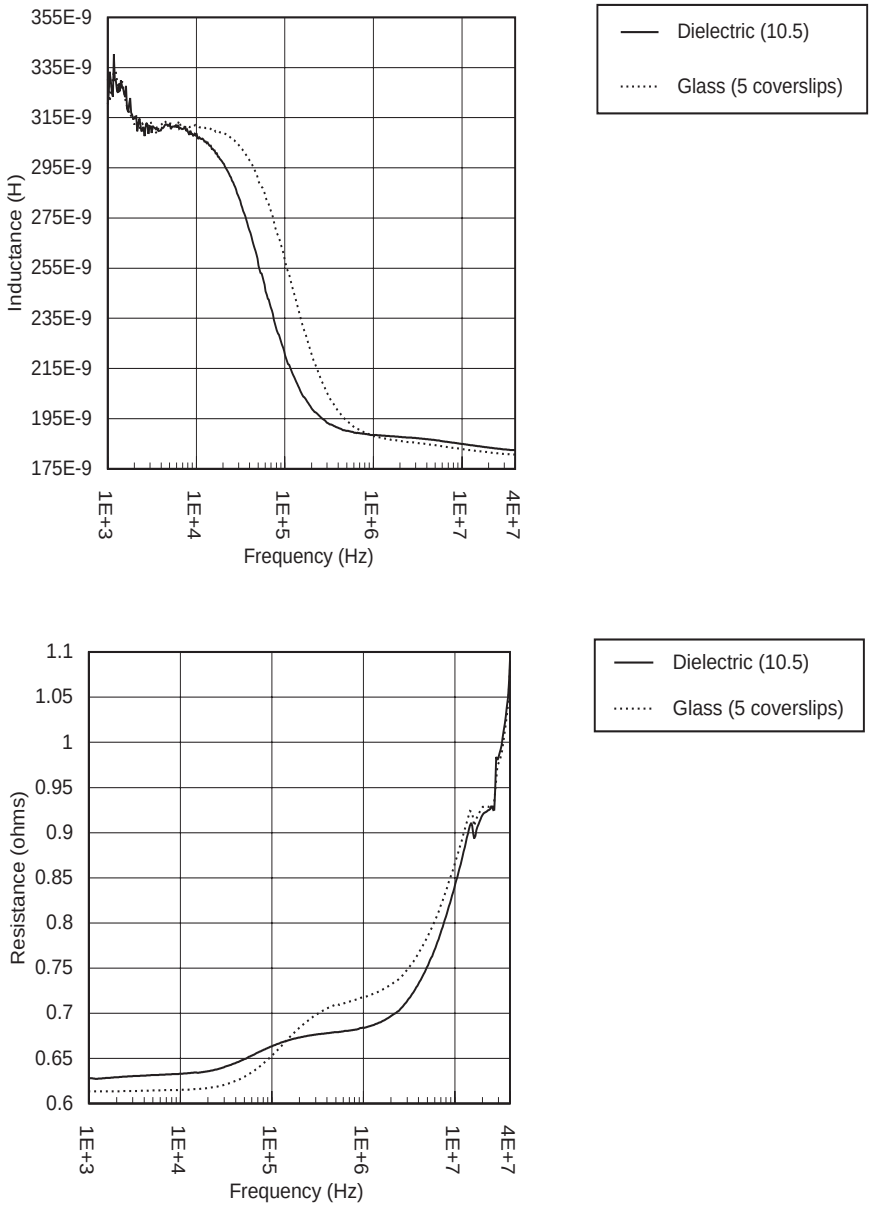


**Fig. (2-17): Inductance and resistance graph for different dielectrics.**

As can be seen from the graphs above, the effect of a different dielectric is not significant. This experiment shows that the dielectric constant of the lubricant (between the

bearing and bearing pad) would not affect the performance of the sensor.

### 2.7.0 Effect of change in resistance of Metal Plate

To determine the effect of a change in resistance of the metal plate on the sensor performance, the inductance of the coil and plate system were measured for metal plates of different resistance. In one case the original copper PCB was used and in the other a thicker brass plate (of lower resistance) was placed at the same distance away from the coil. The results for the experiment are shown below in Fig. (2-18).

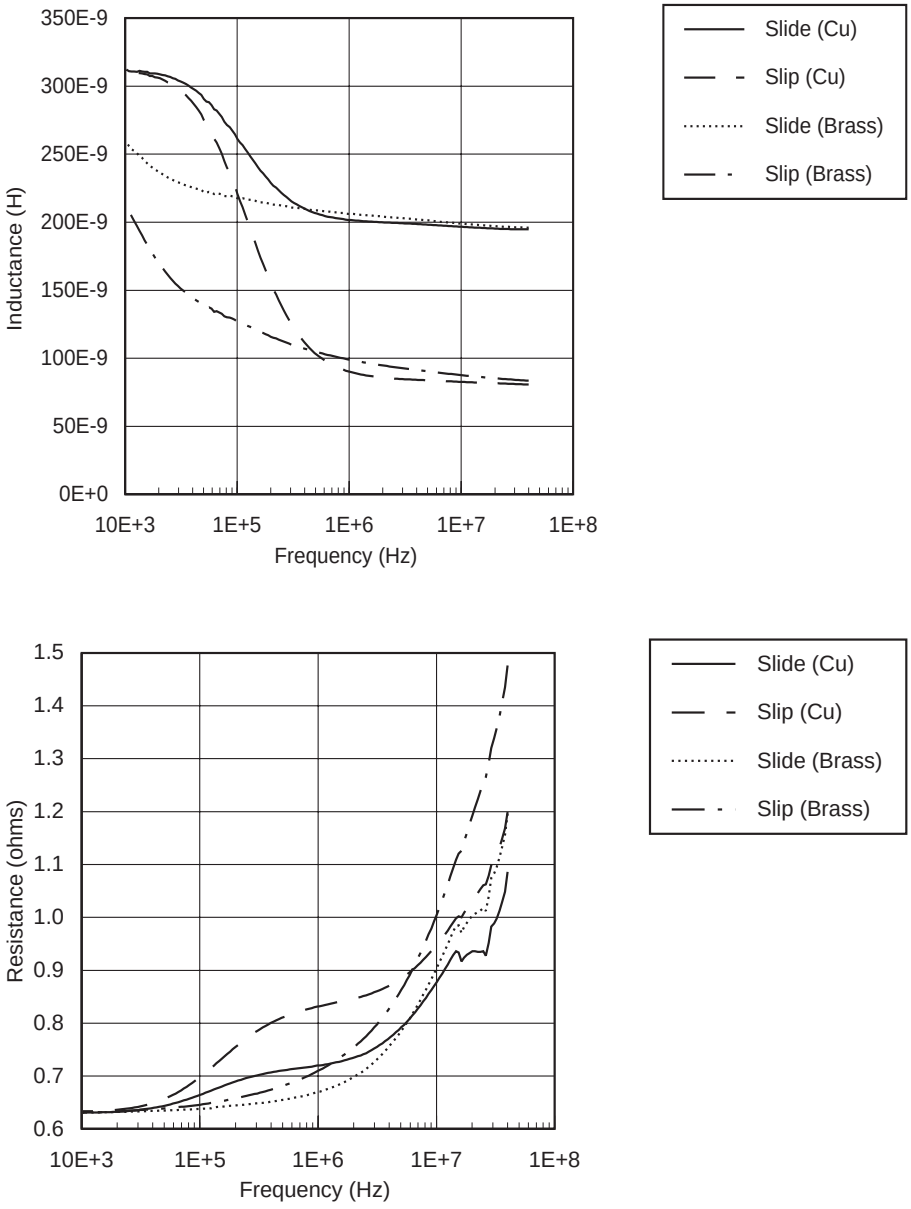


**Fig. (2-18): Inductance and resistance graphs for metal plates of different resistances.**

As can be seen from the inductance graph, the lower resistance of the brass plate

affects the response in the low frequency region. In the higher frequency region the inductance settles to the same value as in the case of the copper plate. This is due to the fact that at lower frequencies the resistive nature of the coil is the dominant factor. At higher frequencies (when $\omega L > R$) the inductive nature of the coil is a dominant factor. In the resistance graph, the “bumps” in the two plots for the brass plate are missing. This is because the increase in resistance due to the proximity effect dominates the increase in resistance due to the metal plate (as explained in Section 2.4.0 on p.32).

## 2.8.0 The Scaling Issue

The spiral coil fabricated on the copper PCB had the dimensions:

$l_1 = l_2 = 1$ cm
width of segment (w) = 0.03 cm
distance between segments (d) = 0.03 cm
thickness of segment (t) = 0.0017 cm
number of segments (n) = 28.

However, the actual coil to be fabricated for a micromachined sensor would need to be much smaller. This means that the inductance and the resistance of the coil will change since these are dependent on the geometry of the coil. In the following discussion, the coil is designed for micromachining by consideration of the effect of the effect of the size parameters on the inductance and resistance.

### 2.8.1 Scaling number of segments (n)

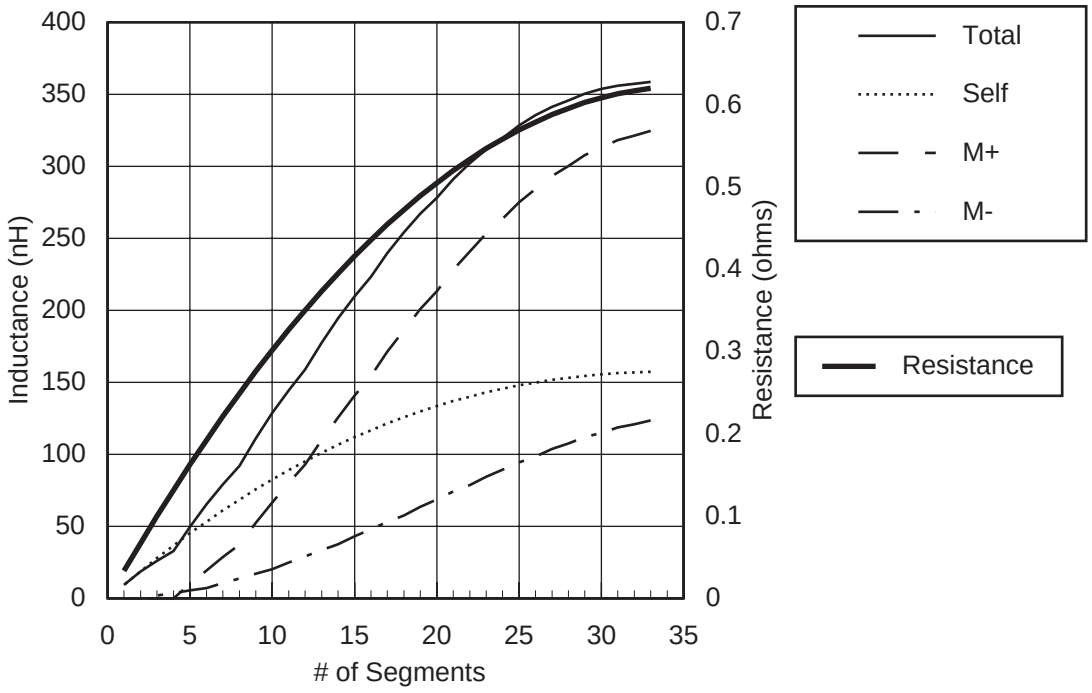


**Fig. (2-19): Scaling the number of segments (n) of the coil.**

As can be seen from Fig. (2-19), as the number of segments increase, the resistance and the inductance of the coil increases. The slope of both the resistance and inductance decreases as the number of segments increase due to the fact that each incremental segment is shorter than the previous (because we are adding segments spiralling in). The contribution of the positive mutual inductance (M+) between segments towards the total inductance of the coil increases rapidly with the increase in the number of segments. Note that all other dimensions for the coil are as stated above.

### 2.8.2 Scaling of distance between segments (d)

Shown in Fig. (2-20) and Fig. (2-21) is the effect on the inductance and the resistance as the distance between the segments increases.

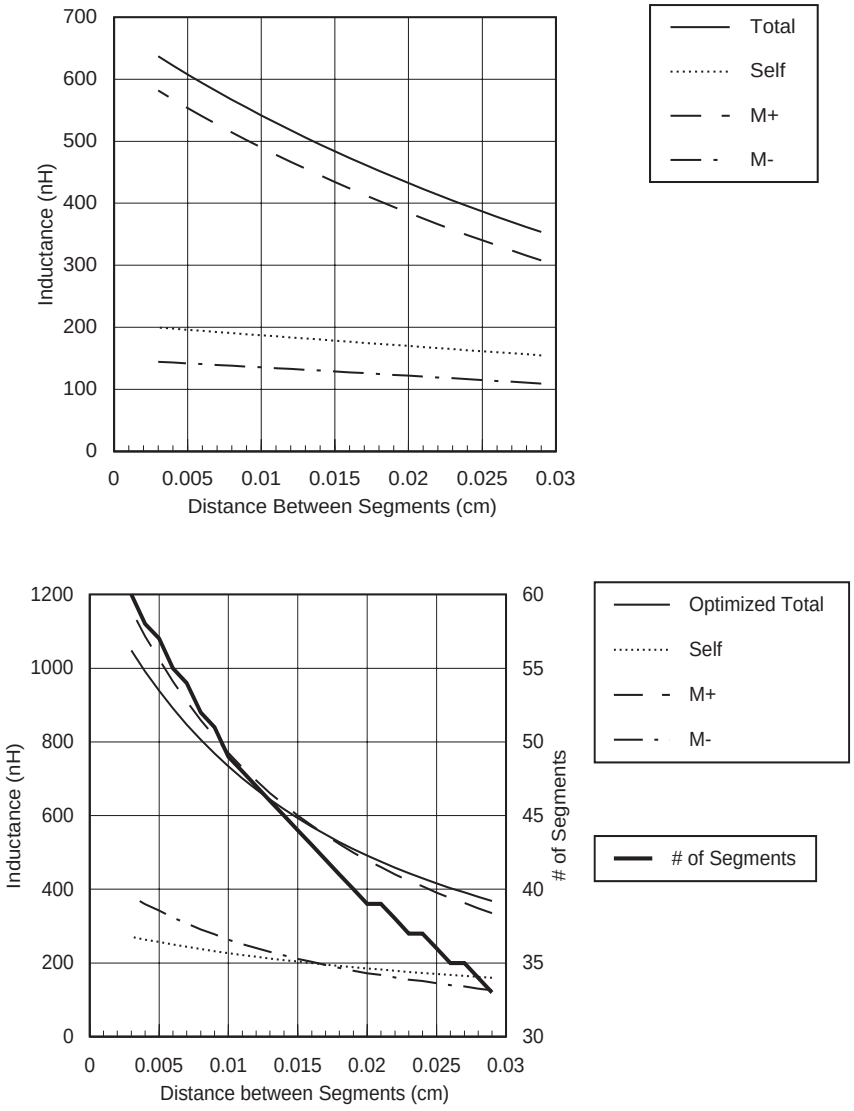


**Fig. (2-20): Effect of scaling the distance between segments on inductance of the coil (unoptimized and optimized).**

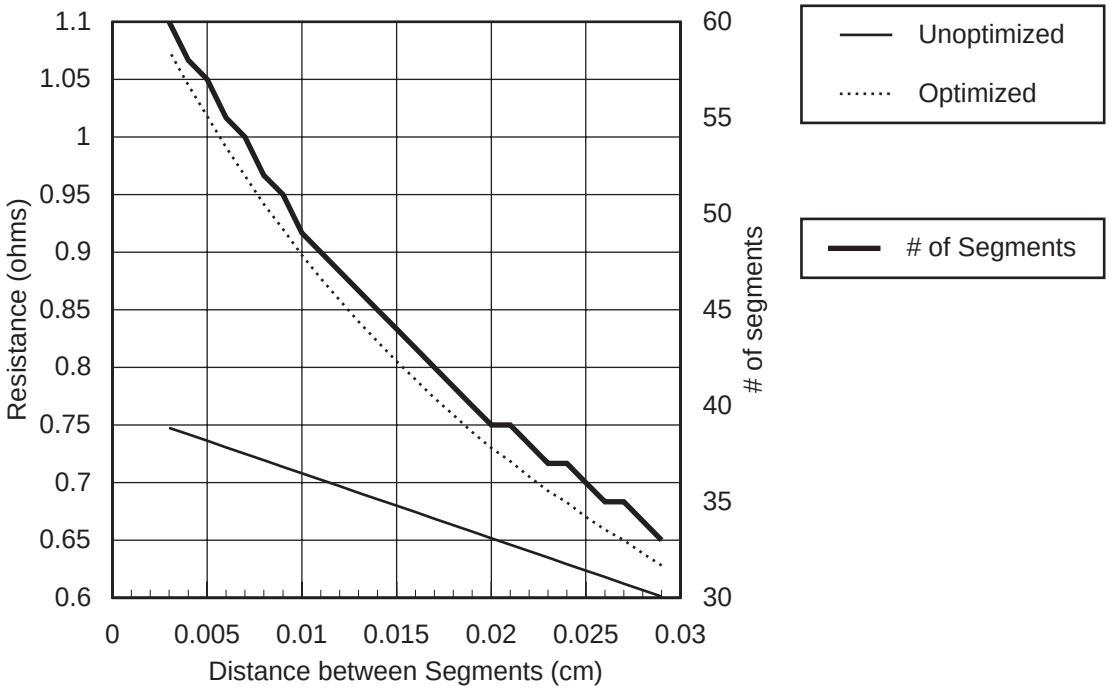


**Fig. (2-21): Effect of scaling of distance between segments on the resistance of the coil (unoptimized and optimized).**

The inductance and the resistance increase with the decrease in the distance between the segments. In both the cases the graphs also show the “optimized” coil for the given distance between the segments. By an optimized coil we mean a coil with the maximum number of segments for the given dimensions of w, t, d, $l_1$ and $l_2$. For the inductance graphs, it can be seen that the inductance increases more rapidly with decrease in the distance between segments in the optimized case. Also, as before, the positive mutual inductance between the segments contributes to a large portion of the total inductance of the coil. For the resistance graph the unoptimized resistance increases slightly with decrease in distance between segments due to the slight increase in path length. The optimized coil shows a sharper increase in resistance due to the increase in

path length due to the increase in the number of segments.

### 2.8.3 Scaling of width of segment (w)

Shown in Fig. (2-22) and Fig. (2-23) is the effect on the inductance and the resistance as the width of the segments decreases.

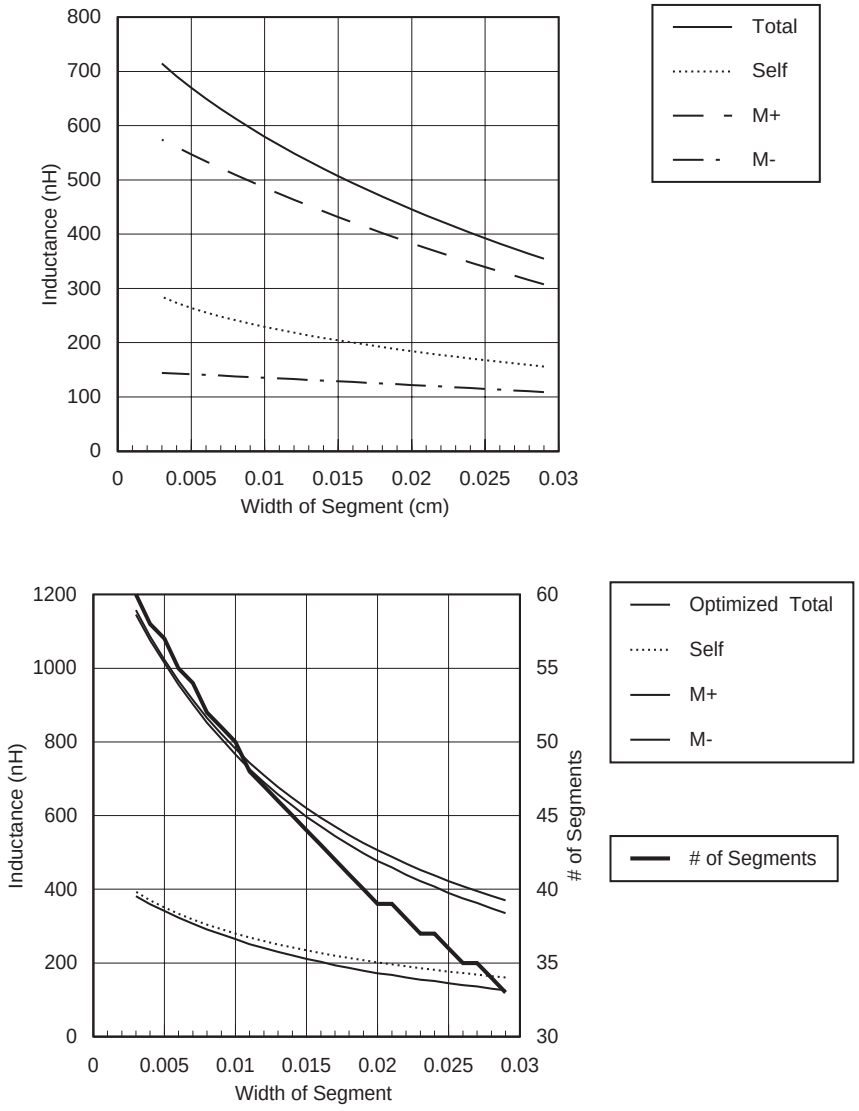


**Fig. (2-22): Effect of scaling the width of the segment on the inductance of the coil (unoptimized and optimized)**

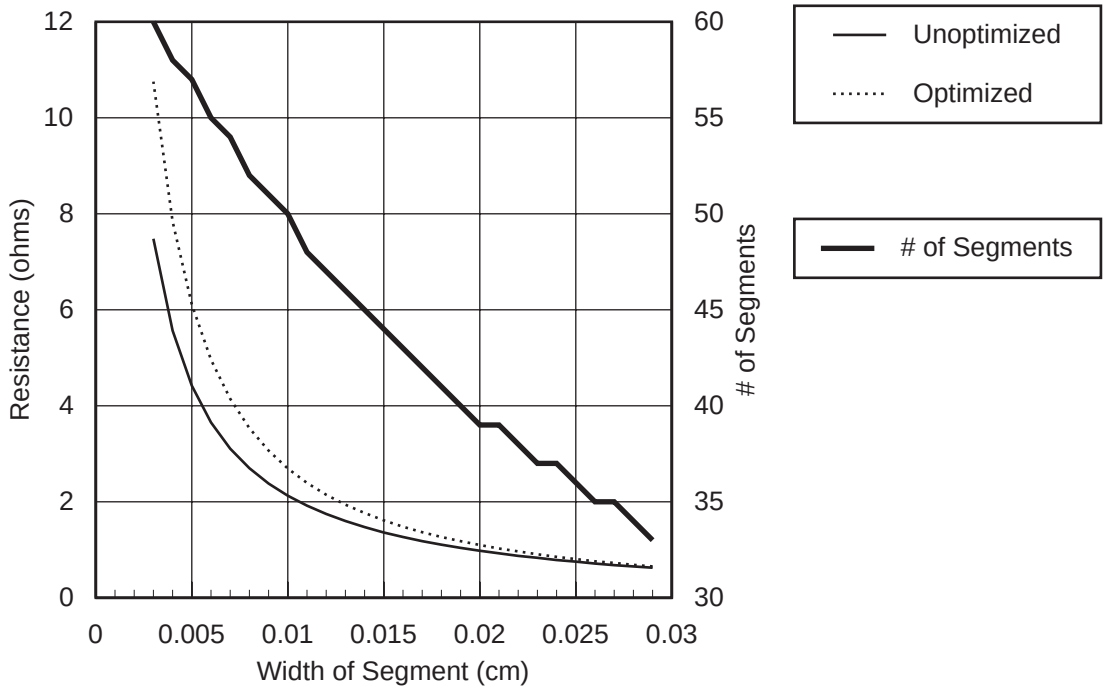


**Fig. (2-23): Scaling of the width of the segment (resistance)**

As can be seen from the inductance graph, the inductance increases with a decrease in the width of the segments. Also compared to the graph for the decrease in the distance between the segments, the change of width affects the inductance a little more than the decrease in distance between segments. The effect of the change in width, however, is a lot more drastic on the resistance graph. The resistance increases almost by a factor of $\frac{1}{width}$ with the decrease in the width of the segments. Again, in both the cases, the graphs also show the optimized coil for the given width of the segments. By an optimized coil we mean a coil with the maximum number of segments for the given dimensions of w, t, d, $l_1$ and $l_2$.

### 2.8.4 Total Coil Scale

In order to see the combined effect of the change in the width of the segments (w), the distance between the segments (d), the length of outer segments ($l_1$, $l_2$) and the thickness of the coil (t), the following scaling rule was used:

$l_1 = l_2$ (where 0.1 cm < $l_1$ < 1 cm)
$d = w = al_1$
$t = bl_1$,

where ‘a’ and ‘b’ are constants. The scaling of the width of the segment, w, has been linked to the length of the segments, l, since Grover’s model assumes that the width of the segment is very small compared to the length. Hence if the length is scaled, the width should be scaled accordingly for the model to be valid. The scaling of the distance between segments is driven by two opposing factors. By decreasing the distance between segments, we can fit more turns of the coil (needed for higher inductance) into the same area but this causes problems in the fabrication (lithography) since the minimum space is usually larger than the minimum line width. By keeping the width of the segment equal to the spacing between segments, a compromise between the two factors can be reached. The thickness of the segment is also linked to the width of the segment since a low aspect ratio ($\frac{thickness}{width}$) is desirable for good step coverage of metal (during metallization) and etching.

For the graphs that follow, a = 0.03 and b = 0.017. These numbers have been chosen so as to maintain the ratios of the large coil fabricated on the PCB. Note that the trends shown in the graphs are independent of the exact values of ‘a’ and ‘b’ as long as w << l (for Grover’s model). Since the number of segments depends upon the ratio of $l_1$ to (d+w), this number is a constant (28 segments) with the scaling rule stated above.

Shown below in Fig. (2-24) is the effect of a total coil scale on the inductance and resistance of the coil. As can be seen from the graph the inductance decreases almost linearly for a decrease in the dimensions of the coil while the resistance increases by a factor of $\frac{1}{length}$ with the same change in dimensions. This means that the Q factor of the coil ($Q = \frac{\omega L}{R}$) decreases as the coil shrinks in size [15].

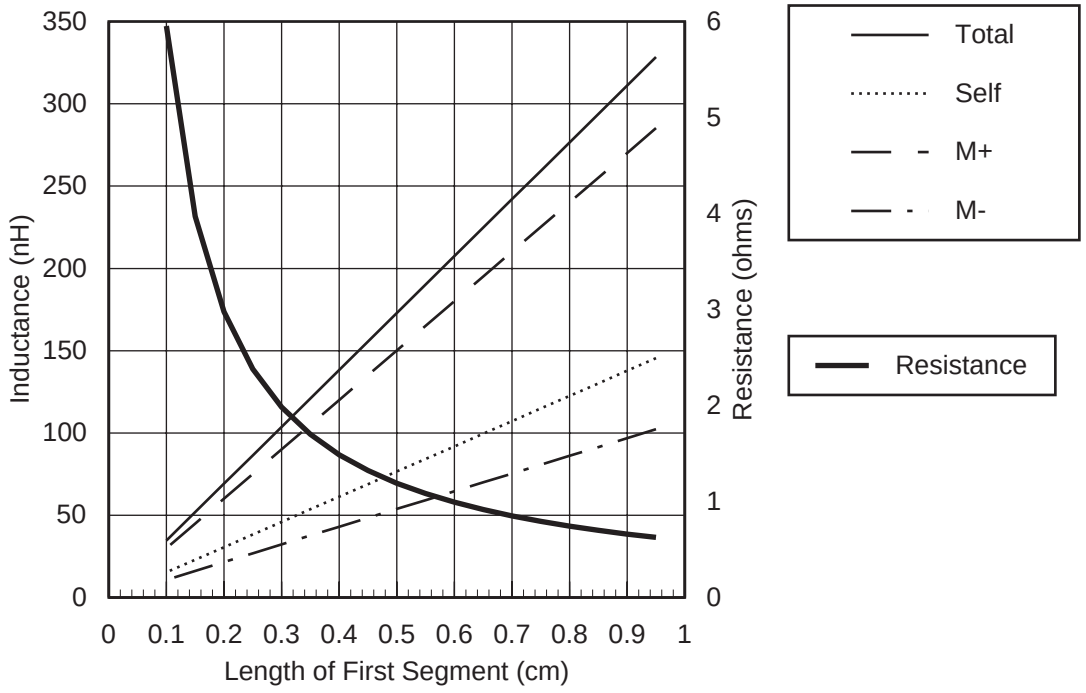


**Fig. (2-24): Effect of a total coil scale on the inductance and resistance of the coil.**

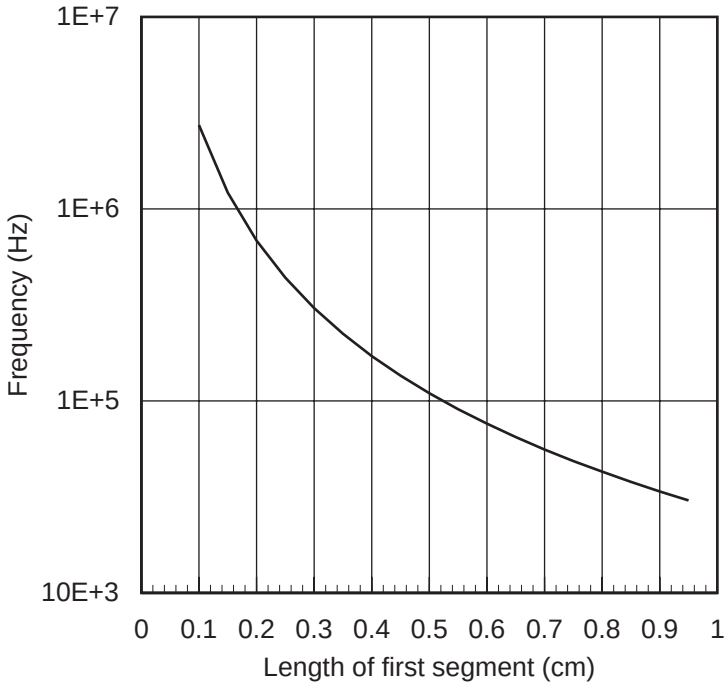


**Fig. (2-25): Graph of the frequency at which the Q-factor equals 1 (or ϖL = R) versus the scaling of the length of the segment.**

The effect of the decrease in the Q-factor of the coil is shown in Fig. (2-25). As can be seen from the graph above, as the length decreases, the frequency ( $frequency = \frac{R}{2\pi L}$ ) at which the Q-factor is equal to 1 (or $\omega L = R$) increases. This implies that for the coil to behave as an inductor, the coil needs to be driven at a frequency in the high megahertz range.

## 2.9.0 Circuits

The single coil transducer can be used with essentially two circuits [13] to function as a proximity sensor.

### 2.9.1 A self excited oscillator test instrument

In this circuit [1][13], the coil forms part of a tank circuit in the self-excited oscillator circuit. Variations in the distance between the coil and the plate would cause a change in inductance causing the tank circuit impedance to change and hence cause a variation in the resonance frequency of the tank circuit and hence the oscillator. Thus a variation in the distance between the coil and the plate would result in a variation in frequency of oscillation.

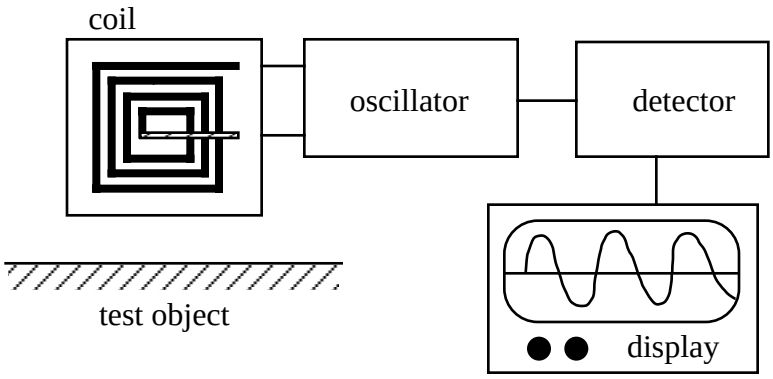


**Fig. (2-26): A self-excited oscillator instrument.**

As the coil is scaled down to integrated circuit levels, the resistance of the coil increases dramatically as explained in section 2.8.4. The magnitude of the impedance of the tank circuit versus frequency shows a peak at the self-resonant frequency of the

tank circuit. As the resistance increases, this peak not only decreases in amplitude but also tends to spread out making the measurement of the resonant frequency very inaccurate.

### 2.9.2 An AC Bridge

A solution to the problem of increase in resistance with scaling is the AC bridge. In this case the coil forms one of the arms of the AC (inductance) bridge [13]. Variations in inductance (due to distance between plate and coil) cause an unbalanced bridge. By adjusting the impedance of the other three arms of the AC bridge, the increase in resistance can be compensated. However for the AC bridge to operate as an inductance bridge the operating frequency would need to be very high for the inductance to dominate over the resistance ($\omega L > R$).

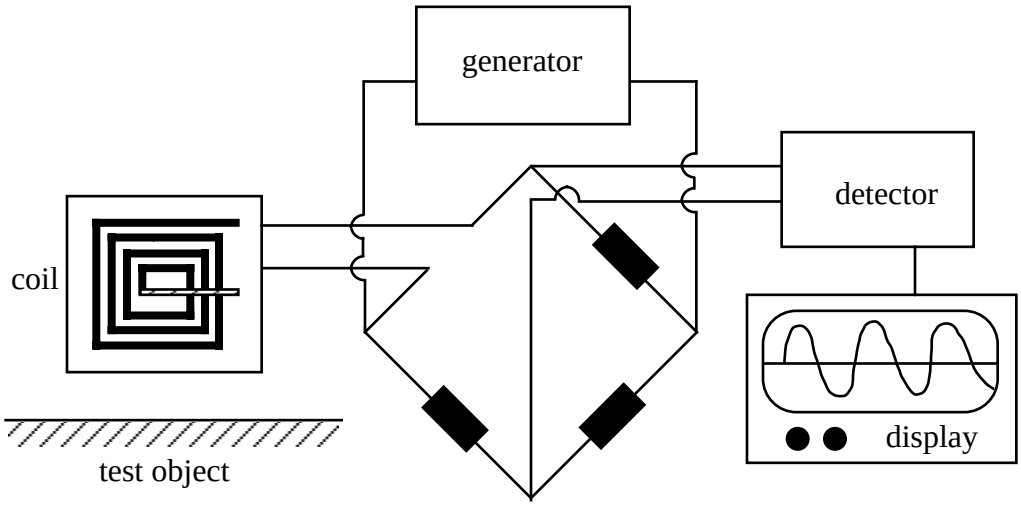


**Fig. (2-27): The AC Bridge circuit.**

## 2.10.0 Summary

In this chapter, methods to calculate the resistance and inductance of coils were discussed. Different coil configurations were explored to obtain the “best results” for the change in inductance with gap. The measured results were explained on the basis of transformer models. The spiral coil was chosen as the best design. The effect of the change in dielectric (between the coil and plate) and the change in plate resistance were explored also. It was seen that the coil is relatively insensitive to these values. The effect of scaling the various dimensions of the coil (number of segments, distance between segments, width of segment and total coil scale) on the resistance and inductance of the coil was also discussed. It was shown that the resistance increases dramatically while the inductance decreases as the coil is scaled to microelectronics levels. Finally, the circuits to be used to drive the coil were shown.

# References


[1] P. Bitsindou, P. Guillaume, G. Delaunay, and G. Villermain-Lecolier, *Detection of Holes, Rivets or Screws Fixed on a Metal Sheet Using a Flat Magnetic Sensor*, Sensors and Actuators (A), vol. 24, pp. 181, 1990.

[2] H. Clergeot, D. Placko, and J. M. Detriche, *Electrical Proximity Sensors*, Sensors and Systems for Advanced Robots, NATO ASI Series, vol. 43, pp. 295, 1986.

[3] H. E. Bryan, *Printed Inductors and Capacitors*, Tele-tech and Electronic Industries, pp. 68, December, 1955.

[4] J. G. Coffin, *The Influence of Frequency upon the self-inductance of coils*, Bulletin of the Bureau of Standards, vol. 2, pp. 275, 2 1906.

[5] H. G. Dill, *Designing Inductors for Thin-film Applications*, Electronic Design, pp. 52, February, 1964.

[6] F. R. Gleason, "*Thin Film Microelectronic Inductors*," National Electronics Conference, Chicago, 1964, pp. 197.

[7] H. M. Greenhouse, *Design of Planar Rectangular Microelectronic Inductors*, IEEE Transactions on Parts, Hybrids, and Packaging, vol. 10, pp. 101, 1974.

[8] F. W. Grover, The calculation of Inductance of Single Layer Coils and Spirals wound with wire of large cross section, Proceedings of the Institute of Radio Engineers, vol. 17, pp. 2053, 1929.

[9] F. W. Grover, *Inductance Calculations: Working Formulas and Tables*, New York: D. Van Nostrand Company, Inc., 1946.

[10] C. R. Paul, Introduction to Electromagnetic Compatibility, New York: John Wiley & Sons, Inc., 1992.

[11] C. Huai-ning, *An Investigation of Microweighing with an Eddy Current Transducer*, Review of Scientific Instruments, vol. 59, pp. 2297, 1988.

[12] D. M. Krafcsik, and D. E. Dawson, *A Closed-form Expression for representing the distributed nature of the spiral inductor*, IEEE Proceedings of the 1986 Microwave and Millimeter-wave Monolithic Circuits Symposium, vol. pp. 87, 1986.

[13] H. L. Libby, *Introduction to Electromagnetic Nondestructive Test Methods*, Wiley-Interscience, 1971.

[14] A. Oliveli, *Optimized Miniature Thin-film Planar Inductors, compatible with Integrated Circuits*, IEEE Transactions on Parts, Materials, and Packaging, vol. 5, pp. 71, 1969.

[15] A. Rand, *Inductor Size vs Q: A Dimensional Analysis*, IEEE Transactions on Component Parts, vol. 10, pp. 31, 1963.

[16] E. B. Rosa, *Calculation of the Self-Inductance of Single-Layer Coils*, Bulletin of the Bureau of Standards, vol. 2, pp. 161, 1906.

[17] E. B. Rosa, *On the Geometrical Mean Distances of Rectangular Areas and the Calculation of Self-Inductance*, Bulletin of the Bureau of Standards, vol. 3, pp. 1, 1907.

[18] P. M. Rostek, *Avoiding wiring-inductance problems*, Electronic Design, pp. 62, December, 1974.

[19] W. H. Hayt, *Engineering Electromagnetics*, McGraw-Hill Book Company, 1988.

[20] A. E. Ruehli, *Inductance calculation in a complex integrated circuit environment*, IBM J. Research and development, 16, pp. 470, 1972.